High Oxygen Permeation in $Ba_{0.95}La_{0.05}FeO_{3-\delta}$ Membranes with Surface Modification

Tetsuya Kida,*,† Subaru Ninomiya,‡ Ken Watanabe,§ Noboru Yamazoe,† and Kengo Shimanoe†

Department of Energy and Material Sciences, Faculty of Engineering Sciences, Kyushu University, Kasuga-Koen, Kasuga, Fukuoka, 816-8580, Japan, Department of Molecular and Material Sciences, Interdisciplinary Graduate School of Engineering Science, Kyushu University, Kasuga-Koen 6-1, Kasuga, Fukuoka 816-8580, Japan, and Sensor Materials Center, National Institute of Materials Science (NIMS), Namiki 1-1, Tsukuba, Ibaraki 305-0044, Japan

ABSTRACT Selective oxygen separation from air was carried out using ceramic membranes composed of $Ba_{0.95}La_{0.05}FeO_{3-\delta}$. We demonstrated that surface abrasion of $Ba_{0.95}La_{0.05}FeO_{3-\delta}$ membranes led to a significant increase in oxygen permeation fluxes at 700−930 °C because of an increase in surface reaction sites. Abrasion of the oxygen desorption side of the membrane resulted in a higher oxygen permeability than with abrasion on the oxygen sorption side. Moreover, an increase in the area of the oxygen desorption side also increased the oxygen permeability. The results suggest that oxygen permeation through $Ba_{0.95}La_{0.05}FeO_{3-\delta}$ membranes is limited by the desorption of oxygen (surface reaction) and bulk diffusion. Attachment of a porous layer made of $Ba_{0.95}La_{0.05}FeO_{3-\delta}$ to the membrane surface was also effective in increasing oxygen permeability. For example, a high permeation flux of 3.2 $cm^3\ min^{-1}\ cm^{-2}$ was achieved at 930 °C under a He/air gradient for a membrane (0.5 mm thickness) coated with a porous layer (14.4 μm).

KEYWORDS: Perovskite • $BaFeO_3$ • oxygen permeation • surface modification • membranes

INTRODUCTION

Fe-based materials have been widely used as electrochemical catalysts and electrodes for power devices such as solid oxide fuel cells (SOFCs) (1−3), polymer electrolyte fuel cells (PEFCs) (4, 5), Li-ion batteries (6−8), and metal−air batteries (9, 10) because of their high performance and low cost. In particular, Fe-based ABO_3 perovskite-type oxides are promising candidates for electrochemical (1−3, 11, 12) and catalytic (13, 14) applications and are considered as alternatives to materials based on scarce elements such as Pt and Co.

Oxygen permeation phenomena through mixed-conducting perovskite-type oxides have attracted considerable attention for use in oxygen separation membranes and membrane reactors (15−18). Recently, we developed a new oxygen permeable membrane using a Fe-based perovskite-type oxide, $BaFeO_{3-\delta}$ (19, 20). In general, compositional modification of perovskite-type oxides by the substitution of A- and/or B-sites in their crystal lattice leads to an improvement in their electrochemical and catalytic activities as a result of changes in the crystal structure, oxygen deficiencies, and electric and ionic conductivities (21, 22). Indeed, the partial replacement of the Ba- and Fe-sites in $BaFeO_{3-\delta}$ with La and Zr, respectively, improved oxygen permeation properties. This was probably due to an improvement in the oxygen ion conductivity, which results from the stabilization of a cubic structure where oxygen vacancies are disordered, thus enabling oxygen ions to move three-dimensionally in the lattice (19, 20). Among the membranes tested, we found that a La-substituted $Ba_{0.95}La_{0.05}FeO_{3-\delta}$ membrane with a 0.5 mm thickness showed a high oxygen permeation flux at 930°C (20), comparable with that of the well-known Co-based membrane, $Ba_{0.5}Sr_{0.5}Co_{0.8}Fe_{0.2}O_{3-\delta}$ (18). However, harnessing this oxygen permeation for practical oxygen separation from air remains challenging, requiring permeation fluxes greater than 10 $cm^3\ min^{-1}\ cm^{-2}$ due to cost and efficiency considerations.

Oxygen permeation through perovskite-type oxides takes place via a series of steps (surface reaction and bulk diffusion): (1) oxygen sorption in the lattice ($1/2O_2 \rightarrow O^{2-} + 2h^+$; oxygen dissociation), (2) bulk diffusion through oxygen vacancies in the lattice, and (3) oxygen desorption from the lattice ($O^{2-} + 2h^+ \rightarrow 1/2O_2$; oxygen association). Provided that the rate-determining step is the bulk diffusion, oxygen permeation fluxes are expressed by the following Wagner equation:

$$J_{O_2} = \frac{RT\sigma_e\sigma_i}{16F^2L(\sigma_e + \sigma_i)}\ln\left(\frac{P_{O_2,high}}{P_{O_2,low}}\right) \quad (1)$$

where Jo_2 is the oxygen permeation flux, L is the membrane thickness, T is the temperature, R is the gas constant, F is the Faraday constant, σ_e is electronic conductivity, σ_i is oxide ion conductivity, and $Po_{2,high}$ and $Po_{2,low}$ are the oxygen partial pressures at the oxygen feed side (sorption side) and oxygen sweep side (desorption side), respectively. This equation predicts that decreasing the membrane thickness will result in increases in oxygen permeation fluxes. For

* Corresponding author. E-mail: kida@mm.kyushu-u.ac.jp.
Received for review June 17, 2010 and accepted August 24, 2010
† Department of Energy and Material Sciences, Kyushu University.
‡ Department of Molecular and Material Sciences, Kyushu University.
§ National Institute of Materials Science (NIMS).
DOI: 10.1021/am100524k

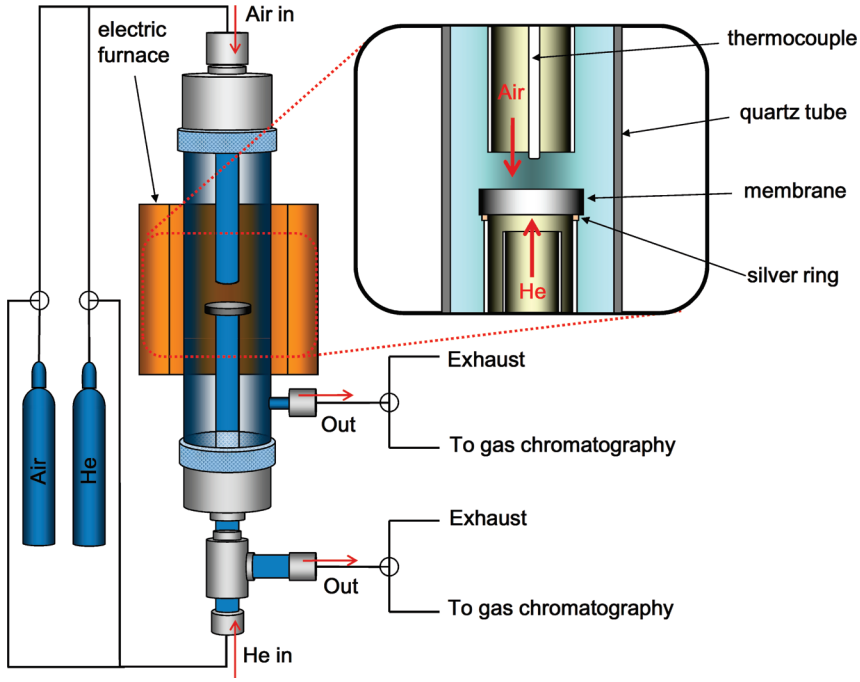

FIGURE 1. Experimental setup for the measurement of oxygen permeation properties of membranes.

some perovskite-type oxide membranes with millimeter thicknesses, such as $La_{0.6}Sr_{0.4}Co_{0.8}Fe_{0.2}O_3$ (23), $La_{0.3}Sr_{0.7}CoO_{3-\delta}$ (24), $Sr_{0.9}Ca_{0.1}CoO_{2.5+\delta}$ (25), and $La_{0.6}Sr_{0.4}CoO_{3-\delta}$-coated $La_{0.7}Sr_{0.3}Ga_{0.6}Fe_{0.4}O_{3-\delta}$ (26), the oxygen permeation fluxes are reported to be linearly related to the inverse of membrane thickness, suggesting that the oxygen permeation in these membranes is limited by the bulk diffusion of oxygen ions. We reported previously that a thin $La_{0.6}Ca_{0.4}CoO_3$ membrane (10 μm) deposited on a porous support showed a high oxygen permeation flux, 1.6 cm^3 min^{-1} cm^{-2} at 930 °C (27, 28). The results indicated the effectiveness of decreasing the membrane thickness to achieve high oxygen permeation rates. However, the permeation fluxes obtained using the thin membrane were still lower than predicted by the Wagner equation. It is suggested that when the membrane becomes sufficiently thin, the surface reaction begins to control the rate of oxygen permeation. Thus, the improvement of the surface reaction rate is critical to obtaining high oxygen permeation fluxes, as noted in the literature (29). It has been reported that surface modification of membranes with porous catalyst layers or by surface-roughening is effective in increasing oxygen permeability (26, 27, 30−32). Lee et al. reported that the deposition of a porous $La_{0.6}Sr_{0.4}CoO_{3-\delta}$ layer on a $La_{0.7}Sr_{0.3}Ga_{0.6}Fe_{0.4}O_{3-\delta}$ membrane increased its oxygen permeability (26). Improvements in the oxygen permeability have also been reported for a $La_{0.6}Ca_{0.4}CoO_3$ membrane coated with a porous $La_{0.6}Ca_{0.4}CoO_3$ layer (27) and a $CaTi_{1-x}Fe_xO_{3-\delta}$ membrane coated with noble metals (32). Teraoka et al. revealed that surface abrasion is also effective in improving the oxygen permeability for a $La_{1-x}Sr_xCo_{1-y}Fe_yO_{3-\delta}$ membrane (31).

We previously reported that the oxygen permeation in $BaFe_{0.975}Zr_{0.025}O_{3-\delta}$ membranes with 0.4−1.0 mm thicknesses is limited by both the surface reaction and bulk diffusion (19). Hence, surface modification is clearly expected to increase the oxygen permeability of $BaFeO_{3-\delta}$-based membranes. In this study, we investigated the effect of surface modification of a $Ba_{0.95}La_{0.05}FeO_{3-\delta}$ membrane on oxygen permeability. The surfaces of the membrane at the oxygen sorption side and/or the desorption side were abraded with emery paper to make the surfaces more porous. We also coated membranes with a porous layer to increase the number of surface reaction sites. The mechanism of oxygen permeation in $Ba_{0.95}La_{0.05}FeO_{3-\delta}$ membranes is also discussed.

EXPERIMENTAL SECTION

Materials Processing. A $Ba_{0.95}La_{0.05}FeO_{3-\delta}$ powder was prepared by a pyrolysis method. Nitrates or acetates of the constituent metals were dissolved in water. The solution was evaporated to dryness at 350 °C, and the dried powder was calcined at 850 °C for 5 h in air. The calcined powder was ground and crushed in ethanol with a planet-type ball-mill for 15 h. After drying, the ball-milled powders were press-formed at 4.0 MPa into a disk (green body diameter: 2 cm) and then sintered at 1175 °C for 5 h in air. For sintering, the heating and cooling rates were set to 4 and 2 °C min^{-1}, respectively.

The surface of the membranes was abraded with emery paper (# 80). The surface was observed on a field emission scanning electron microscope (FE-SEM; JSM-6340F, JEOL Co., Ltd.). The roughness of the membranes was analyzed using a surface texture measuring instrument (SURFCOM 1400D, Tokyo Seimitsu Co., Ltd.). For the coating of porous layers on the membranes, powders of perovskite-type oxides were prepared by the pyrolysis method. The ball-milled powders were dispersed in ethanol to prepare a suspension (1−3 wt %), and then, a designated amount of the suspension was applied to the $Ba_{0.95}La_{0.05}FeO_{3-\delta}$ membranes. Porous layers were formed after drying and calcination at 1000 °C.

Oxygen Permeation Measurements. Oxygen permeation fluxes through the membranes were measured using an apparatus shown schematically in Figure 1. The membrane was fixed to a quartz tube by welding with a silver ring at 960−965 °C. For permeation tests, synthetic air (200 cm^3 min^{-1}) and He (150 cm^3 min^{-1}) were flowed to each side of the membranes,

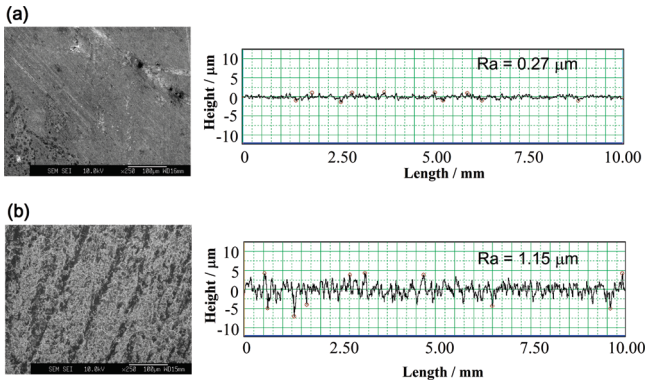

FIGURE 2. SEM-images of a membrane before (a) and after (b) surface abrasion, together with the corresponding roughness profiles.

respectively. The oxygen concentration in the He feed flow was below 0.05 ppm. The amount of oxygen passing through the membrane from the air side (sorption side) to the He side (desorption side) was monitored with a thermal conductivity detector connected to a gas chromatography system. The measurement was performed at 700−930 °C.

RESULTS AND DISCUSSION

Effect of Surface Abrasion. Figure 2 shows FE-SEM images of the surface of a membrane before and after surface abrasion. The surface of the as-fabricated membrane was almost flat, without large pores or large deposits. However, after abrading, the surface became rather porous. The change in the surface porosity was confirmed by measuring surface roughness profiles, as displayed in Figure 2, which shows that the average roughness (Ra) increased from 0.27 to 1.15 μm after surface abrasion.

Four types of membranes were fabricated with and without surface treatment, as shown schematically in Figure 3. Membrane A was an as-fabricated membrane, without surface modification. For Membranes B and C, the surfaces at the oxygen sorption side and the desorption side were treated, respectively (Figure 3b,c), while for Membrane D (Figure 3d) both sides were treated. Figure 4 shows the oxygen permeation fluxes of the four membranes with 0.5 and 0.67 mm thicknesses as a function of temperature (700−930 °C). When the sorption side was treated, almost no increase in the oxygen permeability was observed (Membrane B). On the other hand, the membrane in which the desorption side was treated (Membrane C) showed increased oxygen permeation fluxes in comparison to the membrane fabricated without treatment (Membrane A). This behavior was also observed for membranes with different thicknesses (0.5 and 0.67 mm). In addition, a decrease in membrane thickness improved oxygen permeability. The results clearly indicate that the rate-determining steps for oxygen permeation in the $Ba_{0.95}La_{0.05}FeO_{3-\delta}$ membrane are the desorption of oxygen from the lattice (oxygen association reaction) and bulk diffusion. Note that, for the membrane in which both the desorption and sorption sides were treated (Membrane D), greater increases in the oxygen permeation fluxes were observed. If the rate of oxygen desorption is low and the rate of oxygen bulk diffusion is high enough, oxygen incorporated in the lattice cannot be

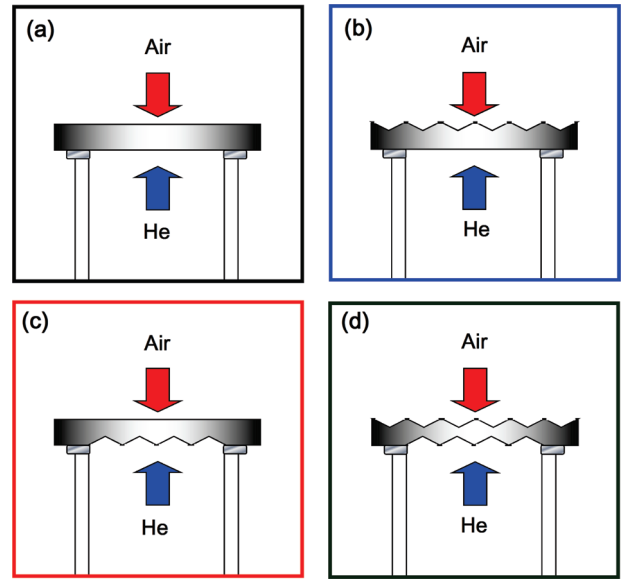

FIGURE 3. Schematics of oxygen permeation membranes with and without surface abrasion: (a) as-fabricated membrane (Membrane A), (b) membrane with the oxygen sorption side treated (Membrane B), (c) membrane with the oxygen desorption side treated (Membrane C), and (d) membrane with the oxygen sorption and desorption sides treated (Membrane D).

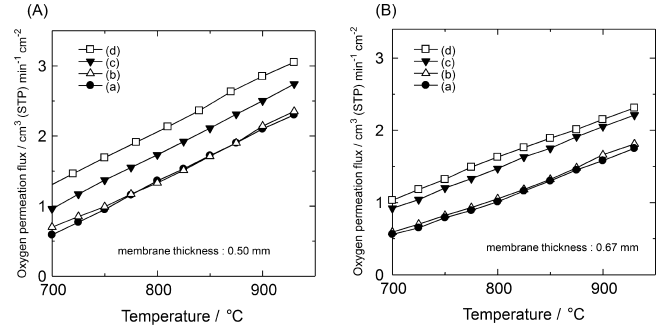

FIGURE 4. Temperature dependence of oxygen permeation fluxes through membranes with different thicknesses (A) 0.5 and (B) 0.67 mm: (a) Membrane A, (b) Membrane B, (c) Membrane C, and (d) Membrane D.

efficiently desorbed from the desorption side. Thus, it is suggested that an increase in the rate of oxygen desorption also led to an increase in the rate of sorption of oxygen in the lattice, thereby increasing the oxygen permeation fluxes when both sides were treated. In particular, the surface treatment effect was more pronounced for thinner membranes (0.5 mm). It is reasonable to conclude that for thinner membranes the surface reaction tends to govern oxygen permeation, because the rate of bulk diffusion of oxygen is high in thin membranes. Thus, the results indicate the effectiveness of surface abrasion for improving oxygen permeability in thin membranes.

To obtain further experimental evidence that supports the above discussion, the effect of membrane desorption area on oxygen permeation flux was investigated. In the experimental configuration used, the apparent oxygen desorption area at the lower side of the membrane (0.77 cm^2) was smaller than the apparent sorption area at the upper side (1.70 cm^2). In this case, oxygen permeates from the upper side to the lower side, as shown in Figure 1. Thus, reversing

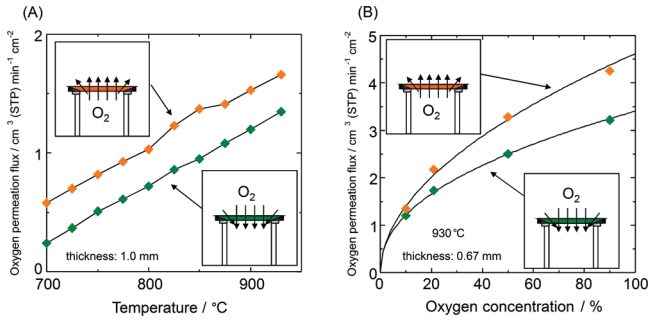

FIGURE 5. Dependence of oxygen permeation fluxes through Membrane A on (A) temperature and (B) oxygen concentration, before and after reversing the air flow direction.

the oxygen permeation direction (air flow direction) can swap the oxygen desorption area for that of oxygen sorption. Figure 5A shows the oxygen permeation fluxes of an as-fabricated membrane as a function of temperature before and after reversing the air flow direction, together with the corresponding schemes of the oxygen permeation direction. The oxygen permeation fluxes significantly increased when oxygen permeated from the lower side (smaller area) to the upper side (larger area). This clearly indicates that increasing the oxygen desorption area resulted in an increase in the oxygen permeability. We also investigated the effect of the feed gas oxygen concentration on oxygen permeation flux. The oxygen permeation fluxes at 930 °C increased with increasing oxygen concentration, as shown in Figure 5B. In particular, at higher concentrations, the oxygen permeability was significantly increased by flow reversal. It is suggested that an increase in the oxygen desorption area likely expanded the oxygen sorption capacity of the membrane. The above results confirm that bulk oxygen diffusion as well as oxygen desorption controlled oxygen permeation in $Ba_{0.95}La_{0.05}FeO_{3-\delta}$ membranes.

Effect of Porous Layer Coating. We also attempted to increase the number of reaction sites and, thus, improve oxygen permeability by coating porous layers composed of $Ba_{0.95}La_{0.05}FeO_{3-\delta}$ onto the membranes. Figure 6 shows FE-SEM images of a porous layer after calcination at 1000 °C. The layer was composed of particles that were about 1 μm and was firmly attached to the membrane. The thickness of the porous layer was controlled from 8.3 to 14.4 μm by changing the concentration of the slurry used for coating. Figure 7 shows the oxygen permeation fluxes of $Ba_{0.95}La_{0.05}FeO_{3-\delta}$ membranes (1.0 and 0.5 mm thicknesses) coated with porous layers deposited on the desorption and sorption sides, as a function of temperature. The membranes with porous layers attached showed similar oxygen permeation fluxes to those of membranes treated with mechanical abrasion. That is, the coating of porous layers had almost the same effect on the improvement in oxygen permeability as mechanical abrasion. Figure 8 shows the dependence of oxygen permeation fluxes on the thickness of porous layers. In this case, porous layers were formed only on the desorption side of the membranes (1.0 mm thickness). The permeation fluxes increased with an increase in the porous layer thickness from 8.3 to 12.4 μm but decreased with a

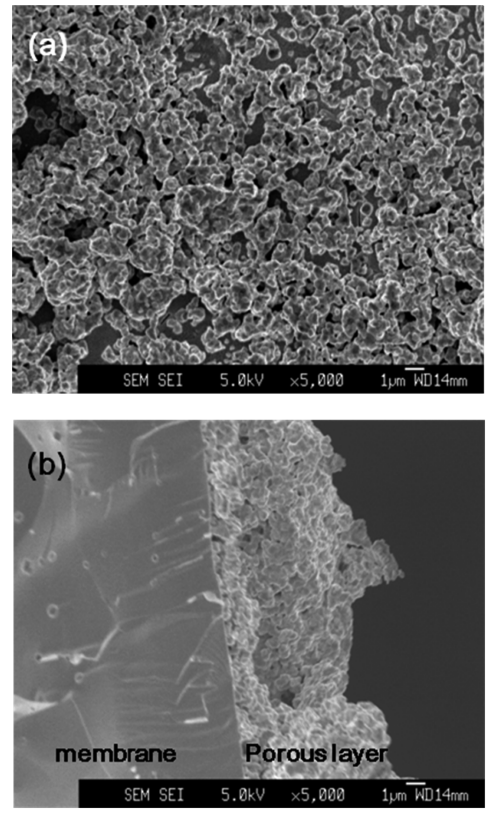

FIGURE 6. (a) Surface and (b) cross-sectional FE-SEM images of a porous layer.

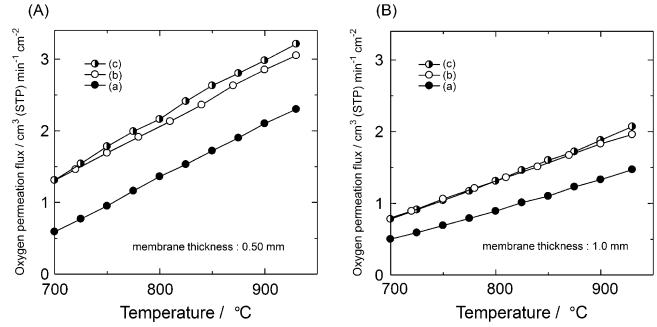

FIGURE 7. Temperature dependence of oxygen permeation fluxes through surface-treated membranes with different thicknesses (A) 0.5 and (B) 1.0 mm: (a) without surface modification (Membrane A), (b) with surface abrasion on both sides (Membrane D), and (c) with porous layers (14.4 μm) on both sides.

further increase in thickness from 12.4 to 14.4 μm. It is probable that increasing the porous layer thickness too much may impede the desorption of oxygen from deep within the porous layer. Thus, the upper part of the porous layers was not effective in assisting oxygen desorption, particularly for thick porous layers. This also suggests that oxygen is mainly desorbed near the interface between the porous layer and the membrane. Control over the microstructure of the porous layer is one feasible way to further increase the oxygen permeation fluxes.

CONCLUSIONS

The surface of $Ba_{0.95}La_{0.05}FeO_{3-\delta}$ oxygen permeation membranes (0.5 mm to 1.0 mm) was abraded with emery paper to increase the porosity of the membrane surface. The

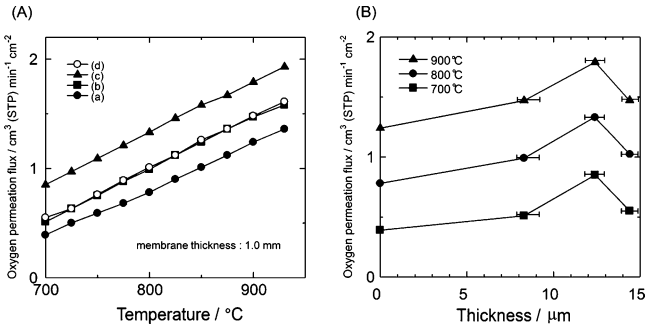

FIGURE 8. (A) Temperature dependence of oxygen permeation fluxes through membranes (1.0 mm) coated with porous layers of different thicknesses on the desorption side: (a) without surface modification (Membrane A) and (b) with a porous layer of 8.3 μm, (c) 12.4 μm, and (d) 14.4 μm. (B) Dependence of oxygen permeation fluxes on porous layer thickness at 700, 800, and 900 °C.

surface treatment led to a significant increase in oxygen permeation fluxes at 700−930 °C because of an increase in the number of surface reaction sites. In particular, oxygen permeability was significantly improved when the porosity of the oxygen desorption side was increased by surface abrasion. The oxygen permeation fluxes were increased by about 30−40% if both sides were treated. Furthermore, increasing the oxygen desorption area of the membrane increased oxygen permeation fluxes. Noting that oxygen permeability can be improved by decreasing membrane thickness, it is suggested that oxygen permeation through $Ba_{0.95}La_{0.05}FeO_{3-\delta}$ membranes is controlled by the desorption of oxygen and its bulk diffusion. Coating membranes with a porous $Ba_{0.95}La_{0.05}FeO_{3-\delta}$ layer (8−14 μm) also led to an increase in oxygen permeation fluxes.

Acknowledgment. The study was financially supported in part by the Kazuchika Okura Memorial Foundation.

REFERENCES AND NOTES

(1) Huang, K.; Lee, H. Y.; Goodenough, J. B. *J. Electrochem. Soc.* **1998**, *145*, 3220–3227.
(2) Simner, S. P.; Bonnett, J. F.; Canfield, N. L.; Meinhardt, K. D.; Shelton, J. P.; Sprenkle, V. L.; Stevenson, J. W. *J. Power Sources* **2003**, *113*, 1–10.
(3) Yamaura, H.; Ikuta, T.; Yahiro, H.; Okada, G. *Solid State Ionics* **2005**, *176*, 269–274.
(4) Lefévre, M.; Dodelet, J. P.; Bertrand, P. *J. Phys. Chem. B* **2002**, *106*, 8705–8713.
(5) Villers, D.; Jacques-Bédard, X.; Dodelet, J.-P. *J. Electrochem. Soc.* **2004**, *151*, A1507–A1515.
(6) Padhi, A. K.; Nanjundaswamy, K. S.; Goodenough, J. B. *J. Electrochem. Soc.* **1997**, *144*, 1188–1194.
(7) Yamada, A.; Chung, S. C.; Hinokuma, K. *J. Electrochem. Soc.* **2001**, *148*, A224–A229.
(8) Okada, S.; Sawa, S.; Egashira, M.; Yamaki, J.-I.; Tabuchi, M.; Kageyama, H.; Konishi, T.; Yoshino, A. *J. Power Sources* **2001**, *97*−*98*, 430–432.
(9) Miura, N.; Hayashi, M.; Hyodo, T.; Yamazoe, N. *Mater. Sci. Forum* **1999**, *315*−*317*, 562–569.
(10) Hang, B. T.; Eashira, M.; Watanabe, I.; Okada, S.; Yamaki, J.-I.; Yoon, S.-H.; Mochida, I. *J. Power Sources* **2005**, *143*, 256–264.
(11) Carbonio, R. E.; Fierro, C.; Tryk, D.; Scherson, D.; Yeager, E. *J. Power Sources* **1988**, *22*, 387–398.
(12) Falcón, H.; Carbonio, R. E. *J. Electroanal. Chem.* **1992**, *339*, 69–83.
(13) Nitadori, T.; Misono, M. *J. Catal.* **1985**, *93*, 459–466.
(14) Zhang, R.; Villanueva, A.; Alamdari, H.; Kaliaguine, S. *J. Catal.* **2006**, *237*, 368–380.
(15) Teraoka, Y.; Zhang, H. M.; Furukawa, S.; Yamazoe, N. *Chem. Lett.* **1985**, *14*, 1743–1746.
(16) Elshof, J. E.; Bouwmeester, H. J. M.; Verweij, H. *Appl. Catal. A* **1995**, *130*, 195–212.
(17) Zeng, Y.; Lin, Y. S.; Swartz, S. L. *J. Membrane Sci.* **1998**, *150*, 87–98.
(18) Shao, Z.; Yang, W.; Cong, Y.; Dong, H.; Tong, J.; Xiong, G. *J. Membrane Sci.* **2000**, *172*, 177–188.
(19) Watanabe, K.; Takauchi, D.; Yuasa, M.; Kida, T.; Shimanoe, K.; Teraoka, Y.; Yamazoe, N. *J. Electrochem. Soc.* **2009**, *156*, E81−E85.
(20) Kida, T.; Takauchi, D.; Watanabe, K.; Yuasa, M.; Shimanoe, K.; Teraoka, Y.; Yamazoe, N. *J. Electrochem. Soc.* **2009**, *156*, E187−E191.
(21) Yamazoe, N.; Teraoka, Y. *Catal. Today* **1990**, *8*, 175–199.
(22) Peña, M. A.; Fierro, J. L. G. *Chem. Rev.* **2001**, *101*, 1981–2017.
(23) Miura, N.; Okamoto, Y.; Tamaki, J.; Morinaga, K.; Yamazoe, N. *Solid State Ionics* **1995**, *79*, 195–200.
(24) Chen, C. H.; Bouwmeester, H. J. M.; Van Doom, R. H. E.; Kruidhof, H.; Burggraaf, A. J. *Solid State Ionics* **1997**, *98*, 7–13.
(25) Miura, N.; Murae, H.; Kusaba, H.; Tamaki, J.; Sakai, G.; Yamazoe, N. *J. Electrochem. Soc.* **1999**, *146*, 2581–2586.
(26) Lee, S.; Lee, K. S.; Woo, S. K.; Kim, J. W.; Ishihara, T.; Kim, D. K. *Solid State Ionics* **2003**, *158*, 287–296.
(27) Watanabe, K.; Yuasa, M.; Kida, T.; Shimanoe, K.; Teraoka, Y.; Yamazoe, N. *Solid State Ionics* **2008**, *179*, 1377–1381.
(28) Watanabe, K.; Yuasa, M.; Kida, T.; Shimanoe, K.; Teraoka, Y.; Yamazoe, N. *Chem. Mater.* **2008**, *20*, 6965–6973.
(29) Bouwmeester, H. J. M.; Kruidhof, H.; Burggraaf, A. J. *Solid State Ionics* **1994**, *72* (PART 2), 185–194.
(30) Lee, T. H.; Yang, Y. L.; Jacobson, A. J.; Abeles, B.; Milner, S. *Solid State Ionics* **1997**, *100*, 87–94.
(31) Kusaba, H.; Shibata, Y.; Sasaki, K.; Teraoka, Y. *Solid State Ionics* **2006**, *177*, 2249–2253.
(32) Figueiredo, F. M.; Kharton, V. V.; Viskup, A. P.; Frade, J. R. *J. Membrane Sci.* **2004**, *236*, 73–80.

AM100524K